

The Prediction of Small Scale Fadings in Radio Propagation Based on the MR-FDPF Method

D1.2: Progress Report

Meiling Luo, Dmitry Umansky, Guillaume Villemaud, Jean-Marie Gorce

April 4, 2011

Abstract

When compared with statistical models, deterministic channel models possess a higher accuracy because they are based on the theory of electromagnetic propagation. However, the lack of the exact information about the environment, such as furniture and materials, limits the accuracy of deterministic channel models. Especially there are often randomly moving people in the environments of reality, which indicates the random feature of radio channels. Therefore, besides the large scale phenomenon determined by deterministic channel models, we also want to predict the small scale effects in order to comprehensively describe the real radio channels.

MR-FDPF (Multi-Resolution Frequency-Domain Partial Flow) method [1] [2] is a deterministic channel model. It is based on the cellular automata formalism [3]. The electric field strength is obtained by summing the fictitious flows traveling along a regular grid of transmitting lines and experiencing scattering at the nodes of the grid. It has been demonstrated that the MR-FDPF is an efficient and accurate method for predicting the received mean power in indoor environments. In this report we mainly investigate the small scale fadings based on the MR-FDPF method. The small scale fadings can be extracted from the electric field strength predicted with the MR-FDPF method by introducing the SLAC (Stochastic local area channel) model. This report is divided into two main parts: narrow band fading statistics and wide band fadings statistics.

1 Introduction

In the introduction, we present the basic principle of the MR-FDPF method. The theory and implementation of MR-FDPF method are detailed in [1] [2]. MR-FDPF method first discretizes the environment into small pixels and assumes that the electric field corresponding to each pixel in the environment can be divided into four directive flows as shown in Fig. 1 and Fig. 2.

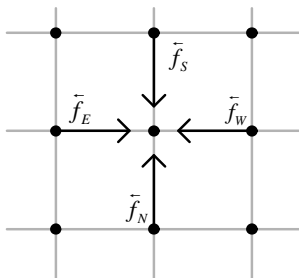


Figure 1: The inward flows associated with each pixel.

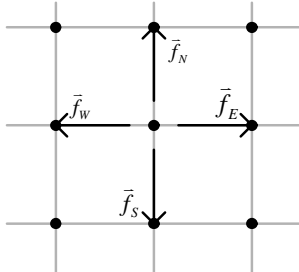


Figure 2: The outward flows associated with each pixel.

The inward flows \vec{f}_d carry energy into the pixel, and on the contrary, the outward flows \vec{f}_d radiate energy outside. The index $d \in \{E, W, S, N\}$ denotes the directions of the flows: East, West, South, and North, respectively. Note that the inward flows of one pixel are outward flows of its neighbour pixels and vice versa. In the frequency domain, the inward flows and outward flows corresponding to each pixel positioned by the radius-vector \vec{r} are bound by the linear frequency domain scattering equation

$$\vec{F}(\vec{r}) = \sum_f (\vec{r}) \vec{F}(\vec{r}) + \vec{S}(\vec{r}) \quad (1)$$

where $\vec{F}(\vec{r})$, $\vec{F}(\vec{r})$ and $\vec{S}(\vec{r})$ are, respectively, the inward, outward and source vectors containing all the four directive flows components. The matrix $\sum_f(\vec{r})$

is the local scattering matrix at the frequency f , which belongs to the signal bandwidth B . After solving the equation (1) the electric field is obtained by summing the inward flows

$$\vec{E}(f, \vec{r}) = \sum_{d=E,W,S,N} \vec{f}_d \quad (2)$$

In order to reduce the computational load, the MR-FDPF method is implemented by using the multi-resolution approach.

2 Extraction of the narrow band fading statistics

In this part, we describe how the fading statistics can be extracted from the predicted electric field strength by the MR-FDPF method.

2.1 Estimation of fading statistics

First, note that since the transmitted signal is always known, the electric field strength predicted with the MR-FDPF method at the position \vec{r} can be equivalently described in terms of the transfer function $H(f, \vec{r})$ of the propagation channel between the transmitting antenna and a virtual receiving antenna located at the position $H(f, \vec{r})$.

At every position \vec{r} , the electric field strength and, consequently, the radio channel transfer function $H(f, \vec{r})$ satisfies the wave equation [3]. Thus, the transfer function $H(f, \vec{r})$ can be legitimately represented by the SLAC model [4] defined as follows

$$H(f, \vec{r}) = \sum_{l=1}^N \alpha_l \exp(j[\Phi_l - \vec{k}_l \cdot \vec{r} - 2\pi f \tau_l]) + w(f, \vec{r}) \quad (3)$$

Each plane wave in (3) is characterized by the constant amplitude $\{\alpha_l\}$, the wavevector $\{\vec{k}_l\}$, the time delay $\{\tau_l\}$, and the phase $\{\Phi_l\}$ which is a realization of the random variable following the uniform distribution over the interval $[0, 2\pi]$. The term $w(f, \vec{r})$ in (3) corresponds to the diffuse wave component [4].

Implicitly, in (3), we assume that the transfer function $H(f, \vec{r})$ as well as the electric field strength predicted by the MR-FDPF method is a realization of the corresponding stochastic process. This assumption can be justified by observing that multiple uncertainties are inherent in modeling any complex propagation scenario. For example, adjustments (corrections) made to the model geographical database, would result in a new realization of the predicted transfer function $H(f, \vec{r})$.

We also presume that the diffuse wave component $w(f, \vec{r})$ in (3) is a realization of a random zero-mean complex Gaussian process uncorrelated with respect to the frequency and the spatial position \vec{r} .

The parameters $\{\alpha_l, \tau_l, \vec{k}_l\}_{l=1}^N$ of the SLAC model (3) are determined by using the well-known space-alternating generalized expectation-maximization

algorithm (SAGE) [5]. Note that under assumptions made above, the estimates $\{\hat{\alpha}_l, \hat{\tau}_l, \hat{k}\}_{l=1}^N$ obtained by the SAGE algorithm asymptotically approach the maximum likelihood (ML) estimates.

The estimated parameters $\{\hat{\alpha}_l, \hat{\tau}_l, \hat{k}\}_{l=1}^N$ of the SLAC model (3) allow determining the statistical properties of the radio channel corresponding to the link between the transmitter and receiver positions. The statistical properties, namely the power delay profile (PDP) $\hat{S}(\hat{\tau}_l)$, the envelope PDF $\hat{f}_R(\rho)$, the FCF $\hat{C}(\Delta f)$, the Rice factor \hat{K} , the mean delay $\hat{\tau}_m$, and the root mean square delay $\hat{\tau}_{rms}$ are calculated as follows [6]:

$$\hat{S}(\hat{\tau}_l) = \sum_{l=1}^N |\hat{\alpha}_l|^2 \delta(\tau - \tau_l) \quad (4)$$

$$\hat{f}_R(\rho) = \rho \int_0^\infty J_0(v\rho) \left[\prod_{l=1}^N J_0(\hat{\alpha}_l v) \right] v dv \quad (5)$$

$$\hat{C}(\Delta f) = \sum_{l=1}^N |\alpha_l|^2 \exp(-j2\pi\tau_l \Delta f) \quad (6)$$

$$\hat{K} = \frac{\max\left((\hat{\alpha}_l)^2\right)}{\sum_{l=1}^N (\hat{\alpha}_l)^2 - \max\left((\hat{\alpha}_l)^2\right)} \quad (7)$$

$$\hat{\tau}_m = \frac{\sum_{l=1}^N \hat{\tau}_l \hat{\alpha}_l^2}{\sum_{l=1}^N \hat{\alpha}_l^2} \quad (8)$$

$$\hat{\tau}_{rms} = \sqrt{\frac{\sum_{l=1}^N (\hat{\tau}_l - \hat{\tau}_m)^2 \hat{\alpha}_l^2}{\sum_{l=1}^N \hat{\alpha}_l^2}} \quad (9)$$

Furthermore, multiple realizations of the transfer function $H(f, \vec{r})$ can be obtained by substituting the estimated parameters $\{\alpha_l, \tau_l, \vec{k}_l\}_{l=1}^N$ into the SLAC model (3).

2.2 Simulation and Measurement

In order to verify the performance of the proposed method, we conduct both the simulation and measurement.

2.2.1 Simulation

In the simulation, CITI lab has been chosen as the indoor propagation scenario where MR-FDPF method is used. The radio coverage map of CITI lab predicted with the MR-FDPF method is presented in Fig. 3. In order to extract the fading statistics, the simulations have been performed at 41 frequencies, at the range 3.477GHz to 3.523GHz, with the frequency step 1.152MHz. The spatial resolution of the MR-FDPF method is 1.4cm. The locations of the transmitter and the virtual receiver are indicated by Tx and Rx, respectively, in Fig. 3. The Rx is a virtual rectangular antenna array consisting of $7 \times 7 = 49$ equidistant elements with spacing equal to 1.4cm. The transmitter power is 17dBm. The SAGE algorithm is applied to the predicted channel transfer function. The number of multiple paths is assumed to be 15.

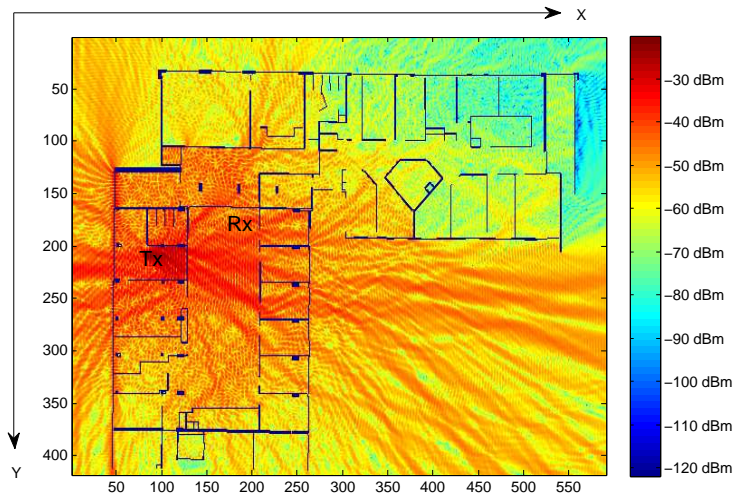


Figure 3: The coverage map predicted with MR-FDPF method.

2.2.2 Measurement

The measurement is conducted at the same position in CITI lab as shown in Fig. 3. The Transmitter includes the arbitrary waveform generator (ESG4438C by Agilent Technology) and the directional antenna (3164-08 by ETS-Lindgren). The vector signal analyser (VSA 89641 by Agilent Technology) is equipped with a 3.5GHz, 6dBi, omnidirectional antenna. The 0.2dB bandwidth of the VSA is 20MHz. Fourteen measurements corresponding to different time instances have been conducted. For each measurement, 9 positions are measured around the Rx in Fig. 3. For each referred receiving position, 4608080 samples are collected during 100ms.

2.3 Results

In order to evaluate the proposed approach, we compare the simulation and measurement results. Fig. 4 presents the comparison of channel impulse responses

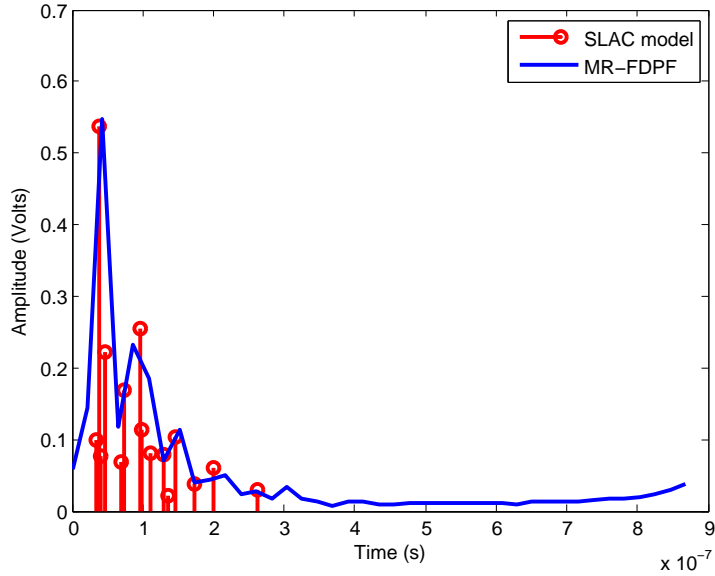


Figure 4: The comparison of the impulse response.

of the SLAC model and that obtained directly by the MR-FDPF method. We can see that they have a good match of each other. The envelope PDFs of the SLAC model estimated by the proposed approach has also been compared to the histogram of channel transfer function in Fig. 5. The histogram of the envelope of the measured channel transfer function is depicted in Fig. 6. The Rayleigh PDF curve is also plotted for comparison reasons. From Fig. 5 we see that the PDF of the SLAC model fits very well the PDF of the MR-FDPF method. Furthermore, both of them match the PDF obtained from the measurements and shown in Fig. 6.

The angle spectrum of the SLAC model is given in Fig. 7. As can be seen from Fig. 7, the estimated angles are grouped near 180 and 0/360 degrees. The group around 180 degrees includes the line-of-sight (LOS) direction, which is approximately equal to 160 degrees. The second group, i.e., the waves with the angles near 0/360 degrees are mainly due to the reflection by the walls behind the Rx.

By the proposed approach, we can also obtain the estimated Rice factor, mean delay, and root mean square delay from the predictions provided by the MR-FDPF method. The results are presented in the Table 1.

The 95% confidence intervals calculated using Chebyshev's inequality are also given in Table I. It can be seen that the simulation results are well located in the 95% confidence intervals of the measurements. In Fig. 8, we show the comparison of the estimated FCF obtained from the SLAC model and the measurements data.

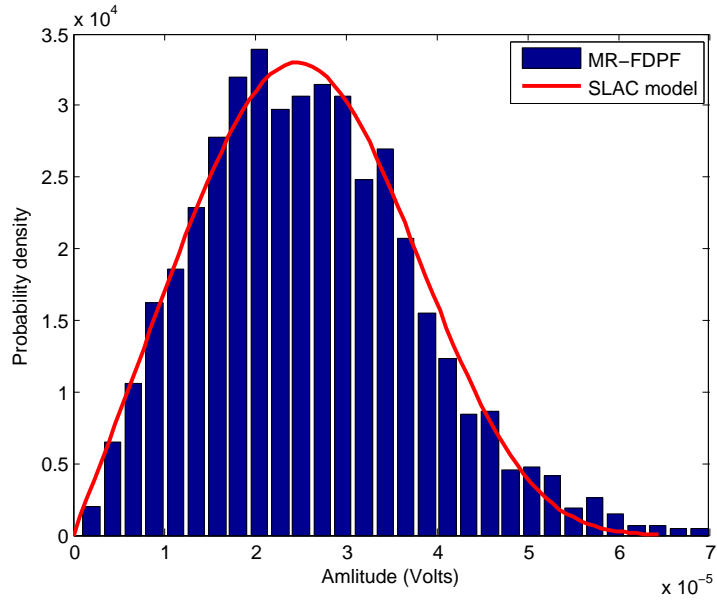


Figure 5: The comparison of the channel envelope PDFs.

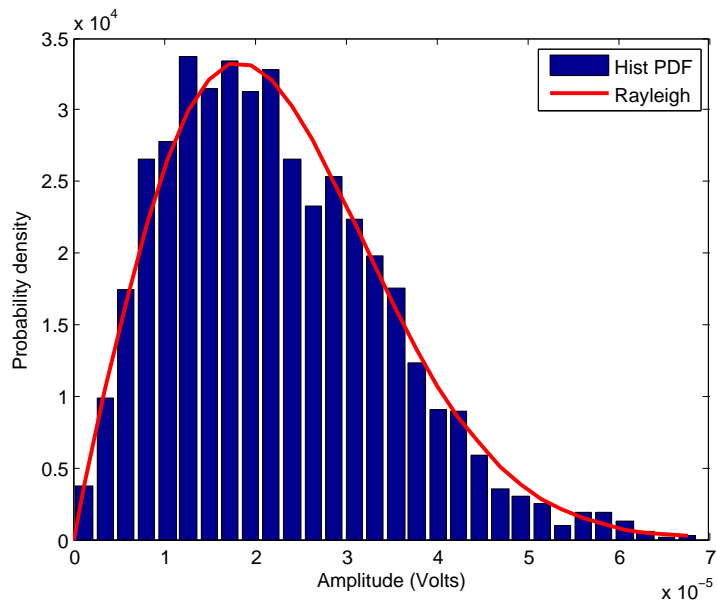


Figure 6: The histogram PDF of measurements.

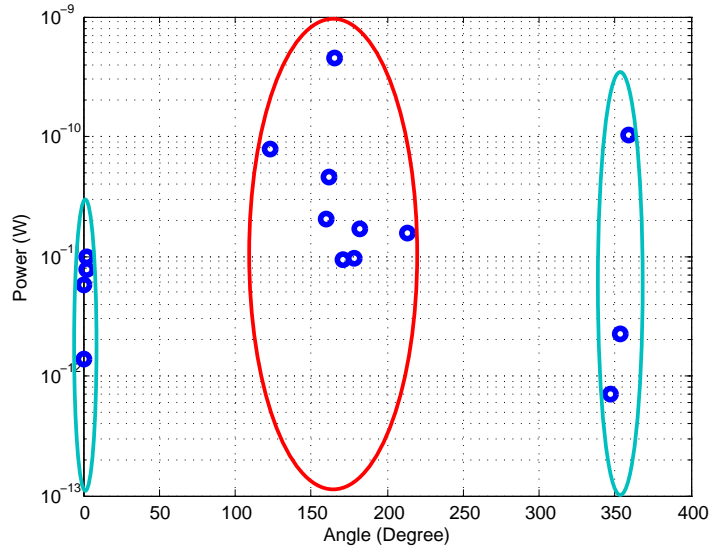


Figure 7: The estimated channel angular power spectrum.

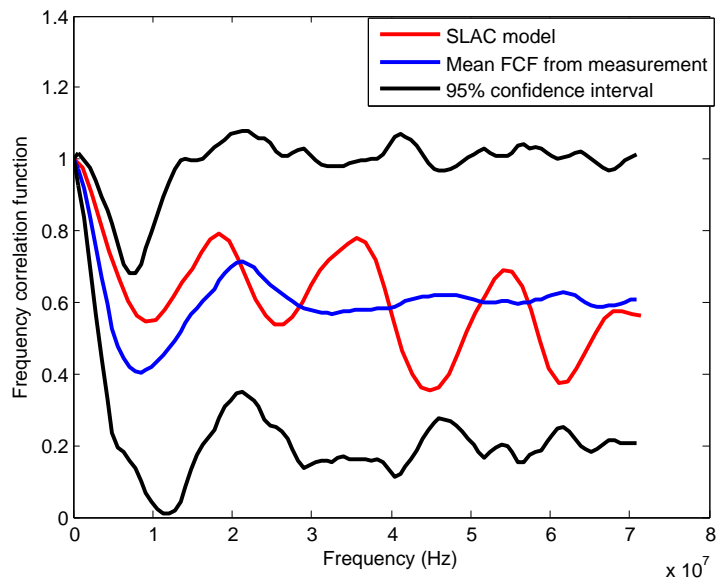


Figure 8: The comparison of FCFs obtained from the SLAC model and measurements.

Table 1: Comparison of estimated values from the SLAC model and measurements

Parameters	From the SLAC model	Mean Values from Measurements	Confidence Intervals
\hat{K}	1.3979	1.4705	[0, 4.9432]
$\hat{\tau}_{rms}$	$3.178 \times 10^{-8} s$	$5.2711 \times 10^{-8} s$	[0, $1.4158 \times 10^{-7} s$]
$\hat{\tau}_m$	$5.7568 \times 10^{-8} s$		

2.3.1 Conclusion

In this part we present how fading statistics of indoor wireless channels can be extracted based on the prediction of electric field provided by the MR-FDPF method. In order to verify the performance of the proposed approach, both the simulations and measurements have been conducted. The comparison of the results obtained from the simulations and measurements demonstrates that the proposed method is efficient in extracting the fading statistics.

3 Wide band fading statistics based on the MR-FDPF method

In order to increase the capacity, future wireless networks will use larger bandwidths. For instance, LTE-Rel 10 proposes to aggregate LTE-Rel 8 sub-bands, in order to reach a bandwidth of up to 100 MHz. Therefore, channel models which characterize large bandwidth are useful in order to study the performance of any new future wireless communications systems. However, most of current approaches, such as IMT-Advanced channels, suppose that fading has homogeneous properties in the working bandwidth (which was in the past in general less than 20 MHz). That is why new models are now needed. In [7] we recently showed that parameters describing the fast fading (such as K -factor, fading depth, number of significant paths, etc.) are bandwidth-dependent and we proposed a model based on a measurement campaign. Bandwidth dependency properties of fading like fading depth was also investigated in [8] for ultra wide band systems. However, except few studies, there is still a lack of measurements available to extract properly all the parameters of the fast fading when moving to large bandwidth and there is currently no general model to define the wide band fast fading due to multiple paths.

Let us notice that the bandwidth dependency variations of the fast fading can be explained by the variations in the received signal, due to the constructive or destructive addition of multiple paths with different phases. These variations depend on the different frequencies since the materials, in the scenario under consideration, behave differently at different frequencies. Furthermore, these variations depends also highly on the scenario. For instance, complex scenarios with many walls and thus more paths, are not expected to have similar multipath fading properties compared to a more open space environment. Since measurement campaigns are time consuming and costly, it would be very useful to be able to estimate the wide band variations of the channel due to multiple paths for a given scenario. Therefore, in this part of the report, we investigate

simulating these variations by using the MR-FDPF method.

Finite difference models such as finite difference time domain (FDTD) are a more and more common approach to simulate the path loss attenuation of a source in a given environment [9]. The main advantage is that they directly solve the Maxwell's equations. Therefore, unlike other common techniques like ray tracing, where the number of rays to compute has to be limited for complexity reasons, finite difference models implicitly take into account all the reflections and diffractions. Furthermore, finite difference methods require to use a small spatial resolution compared to the wavelength, thus leading to a very fine radio coverage allowing to identify very accurately all the different paths. Therefore, since we want to study the wide band variations of the channel due to multiple paths, finite difference methods seem very appropriate for our purpose. At our knowledge, such study was not performed before and we believe finite difference models may be a very interesting technique, for instance for simulating the channel in a given scenario where carrier aggregation is used.

3.1 Scenario and Measurements

To evaluate the performance of our model, we used the measurement campaign corresponding to "I2I stationary" scenario performed at Stanford by Dr. N. Czik [10]

3.1.1 The office scenario

The indoor scenario is a 16m x 34m office environment where 8 transmitters (Tx) and 8 receivers (Rx) are distributed in the building as shown in Fig. 9. All of these transmitters and receivers have omnidirectional antennas which are fixed during the measurement. This environment is a typical office environment, with few closed rooms and open space cubicles. It is made of four main materials, i.e., *concrete* for the main walls, *plaster* for the internal walls, *glass* for the windows and *wood* for the cubicles located in the central part of the scenario.

3.1.2 Channel sounder measurements

The RUSK Stanford radio channel sounder [11] has been adopted to conduct the measurement which is capable of measuring up to 8 x 8 MIMO channels at a center frequency of 2.45 GHz. In the measurement 120 time blocks corresponding to a total time of 32 seconds and 200 frequency bins covering a bandwidth of 70 MHz are recorded. Then, channel sounding measurements characterize the channel matrix for each link. As an illustration, one link is plotted in Fig. 10 where we can see that only minor variations are observed in the time domain (due to static transmitters and receivers) but large variations in the frequency domain (up to 20 dB in this case) are observed. Therefore, Doppler spread can be neglected and the variations can be explained by the wide band multipath fading.

3.2 Finite Difference Simulation

The finite difference propagation tool we uses is the multi-resolution frequency domain ParFlow method (MR-FDPF) detailed in [12]. This approach is a simplification compared to FDTD, in the sense that the fields are considered as



Figure 9: The measurement scenario.

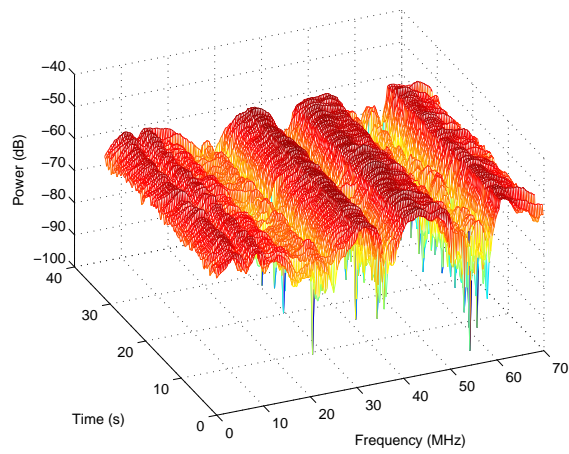


Figure 10: Example of the measured channel time frequency responses for one link.

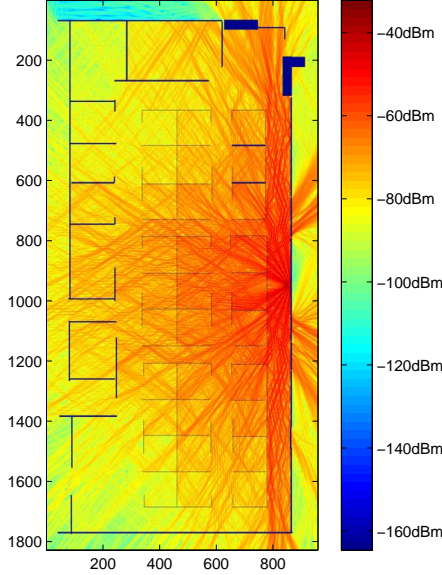


Figure 11: Example of one narrow band radio coverage simulated with MR-FDPF and plotted in dBm.

scalar, instead of having E and H vector fields. The MR-FDPF method firstly discretizes the environment under investigation into small pixels and then implements two main phases: the upward phase and downward phase. The aim of the upward phase is to compute the equivalent source while the aim of the downward phase is to propagate the equivalent source obtained during the upward phase to the pixels. In the implementation a preprocessing and a multi-resolution technique reduce a lot the complexity. For our study, in order to reduce the simulation time, the method is restricted to 2D which was shown to be appropriate in a flat multi floor environment where main propagation effects occur in the horizontal plane, and where vertical effects are compensated for using a proper calibration of materials [12]. In Fig. 11 the computed narrow band radio coverage of one transmitter in the office scenario is plotted. Using this model, the wide band simulation of the received signal is performed by running N narrow band simulations covering the bandwidth under investigation. The resolution of the coverage defined by the size of the each pixel is 2 cm. Therefore, for a given transmitter, our method computes the received signal every 2 cm, for N frequencies.

Note that the 2D approximation due to the consideration of the computational load introduces the prediction error. In order to improve this, a calibration process is introduced [13]. The calibration process is divided into two parts. The first part is to estimate the offset which is defined by:

$$\Delta\Psi = \frac{1}{m} \sum_{k=0}^m (\Psi_{mes}(k) - \Psi_{sim}(k)) \quad (10)$$

where $\Psi_{mes}(k)$ and $\Psi_{sim}(k)$ are the mean powers from measurements and simulations, respectively, and m is the number of samples. The second part is to estimate the attenuation coefficient of the air α_{air} and the set of parameters (n_{mat}, α_{mat}) of each material, where n_{mat} and α_{mat} are the attenuation coefficient and the reflection factor of each material. We define the cost-function Q by the root mean square error (RMSE):

$$Q = RMSE = \sqrt{\frac{1}{m} \sum_{k=0}^m \|\Psi_{mes}(k) - \Psi_{pred}(k)\|^2} \quad (11)$$

where

$$\Psi_{pred}(k) = \Psi_{sim}(k) + \Delta\Psi \quad (12)$$

Then these parameters are obtained by minimizing the cost-function Q . This minimization is solved by the direct search algorithm "DIRECT" by Jones et Al. in [14].

3.3 Results

By wide band simulations of the MR-FDPF method, we obtain the bandwidth dependency variations of the fading characteristics. We compare here the bandwidth dependency variations of the fading characteristics of the links between 3 transmitters (Tx1, Tx2 and Tx3) and 8 receivers from the simulations and measurements in Fig. 12-17. In these figures, the receiving powers are plotted in dBm and the horizontal ordinate is frequency covering 70MHz centered at 2.45GHz. The blue dash lines are fading characteristics of simulations and the red solid lines are those of measurements. Since fading characteristics are very sensitive and have a high level of variations, it is very difficult to verify the fading characteristics obtained from simulations by measurements. However, We can see from these figures that the fading characteristics both from the simulations and measurements display the bandwidth dependency characteristics and the fading depths (FD) of them are very closed which will be analyzed in the following.

3.3.1 Fading depth analysis

FD is an important parameter since it affects a lot the system performance. An accurate knowledge of FD is very useful for the design of reliable communications. It represents how severe the channel fading is. Here we define the FD as:

$$FD = \bar{P}_i - \min(P_i) \quad (13)$$

where P_i are the received powers in dBm, $\bar{\cdot}$ and $\min(\cdot)$ denote the mean and minimum value of its variable, respectively.

In the table 2, we compare the mean FD of the total $8 \times 8 = 64$ links from the measurements and the simulations by the MR-FDPF method. This table show that the mean FD by simulations are very closed to the mean FD by measurements, it means that the MR-FDPF method is capable of simulating fading in the wide band.

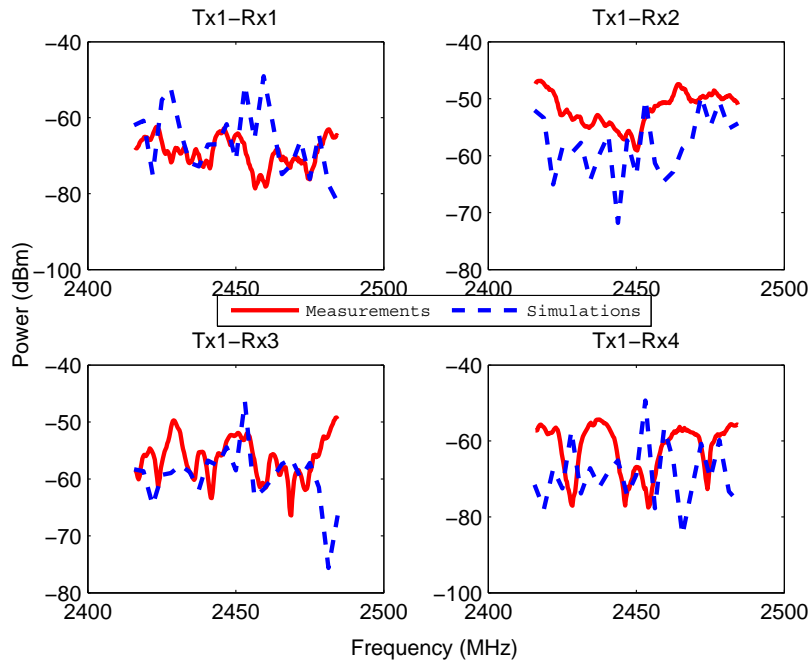


Figure 12: The comparison of the bandwidth dependency variations of the fading characteristics of the links between the Tx1 and the Rx1-4.

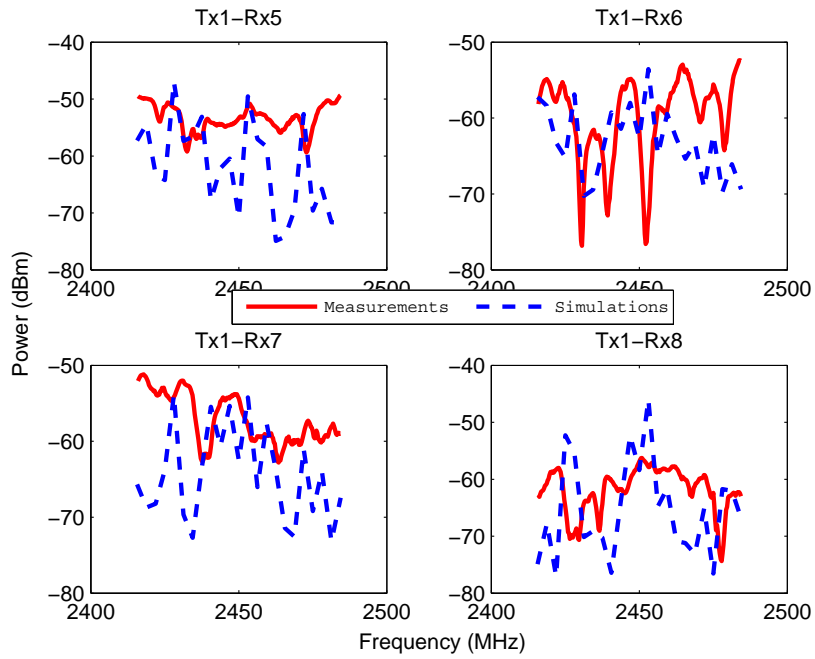


Figure 13: The comparison of the bandwidth dependency variations of the fading characteristics of the links between the Tx1 and the Rx5-8.

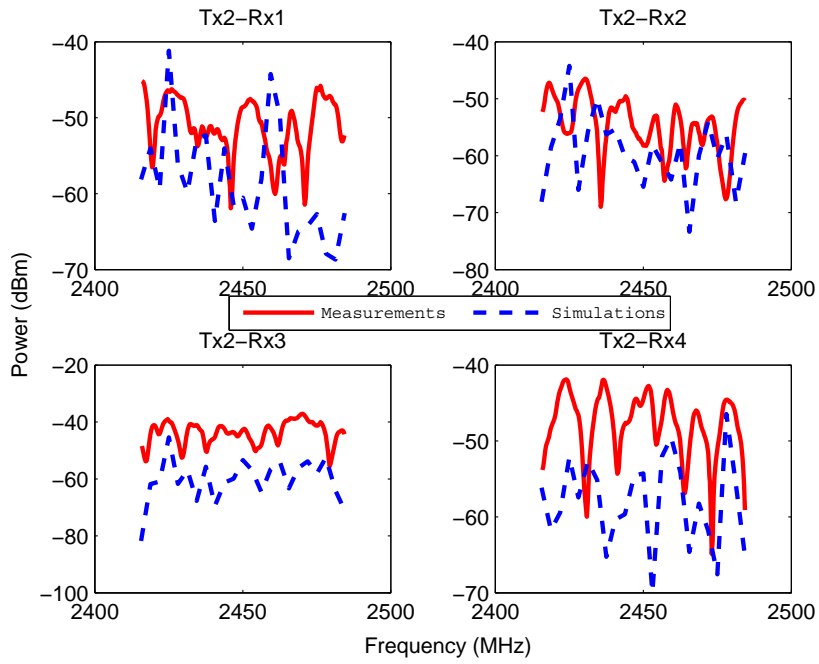


Figure 14: The comparison of the bandwidth dependency variations of the fading characteristics of the links between the Tx2 and the Rx1-4.

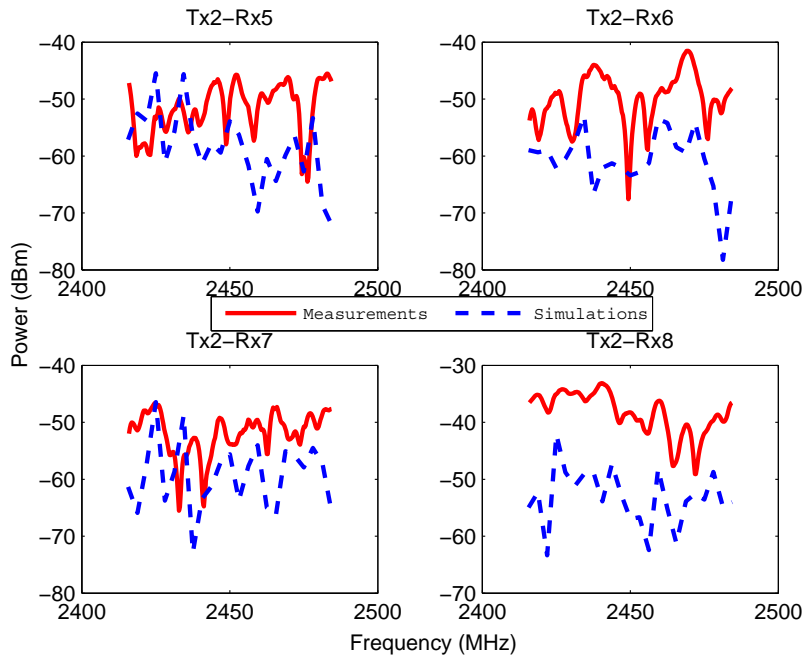


Figure 15: The comparison of the bandwidth dependency variations of the fading characteristics of the links between the Tx2 and the Rx5-8.

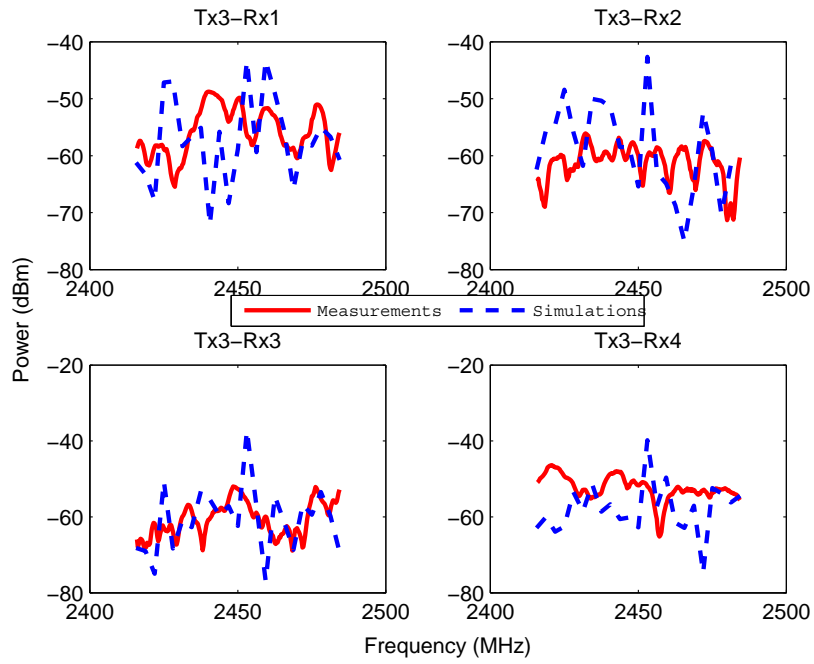


Figure 16: The comparison of the bandwidth dependency variations of the fading characteristics of the links between the Tx3 and the Rx1-4.

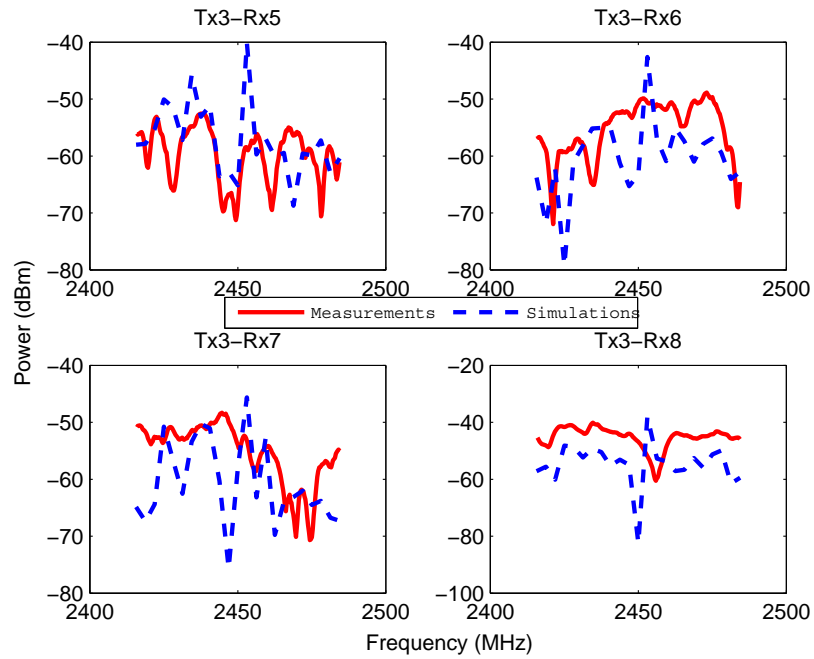


Figure 17: The comparison of the bandwidth dependency variations of the fading characteristics of the links between the Tx3 and the Rx5-8.

Table 2: The comparison of the fading depth from measurements and simulations

Mean	Measurements	Simulation
Mean values of the fading depth	12.6762	15.2606

3.3.2 Study of space variations of fading variations

We also investigate the fading variations by the simulation of MR-FDPF method when moving the Rxs with one pixel distance (2cm) in Fig. 18-19. These two figures show that the fading characteristics can be different even when moving 2cm. Therefore, we know that fading characteristics is very sensitive and it is not possible to get exactly the same fading characteristics at a given point with measurements. For instance, the positions of Tx and Rx are not known at such an accuracy both in measurements and simulations. And in our simulation we did not include furniture which also modifies slightly the directions and amplitudes of the different paths.

3.3.3 Interest of our method

As shown above, the MR-FDPF method is efficient in simulating the fading statistics, but it is important to notice that our technique requires to work at a very fine precision since it requires to know the exact multipaths at a very accurate position. This leads to a high computational load and thus the computation time. For example, with a computer configured by the 4096MB memory, 1066MHz DDR3 Dual Channel, it will take about 7 minutes to finish the simulation of this 16m x 34m environment with 8 transmitters at the spatial resolution of 2 cm. This is the main drawback of the MR-FDPF method when simulating the fading characteristics. In the future, we could further focus on how to improve the MR-FDPF method [15] in order to provide a good trade off between the computation time and the accuracy when extracting the fading statistics.

Also due to the high accuracy requirement for estimating fading characteristics, the finite difference like channel models which can have a very fine accuracy are the unique solution to study the fading characteristics for large bandwidth. The fading characteristics for narrow band systems has already been tackled by the MR-FDPF method in [16] [17]. Here in this report we tackle the fading characteristics for wide band systems.

3.4 Conclusion and Perspectives

In order to meet the use of larger bandwidth, wide band channel models are needed and useful for future wireless communications. In this part of the report, we investigate the bandwidth dependency fading characteristics of the simulation by the MR-FDPF method. In order to verify the simulation results by the MR-FDPF method, we compare them with the measurements conducted at a bandwidth of 70MHz. The comparisons show that our MR-FDPF method is capable for simulating the wide band fast fading characteristics. One thing we should emphasize is that the fading statistics can only be addressed by the finite difference like channel models because they can have a very fine accuracy

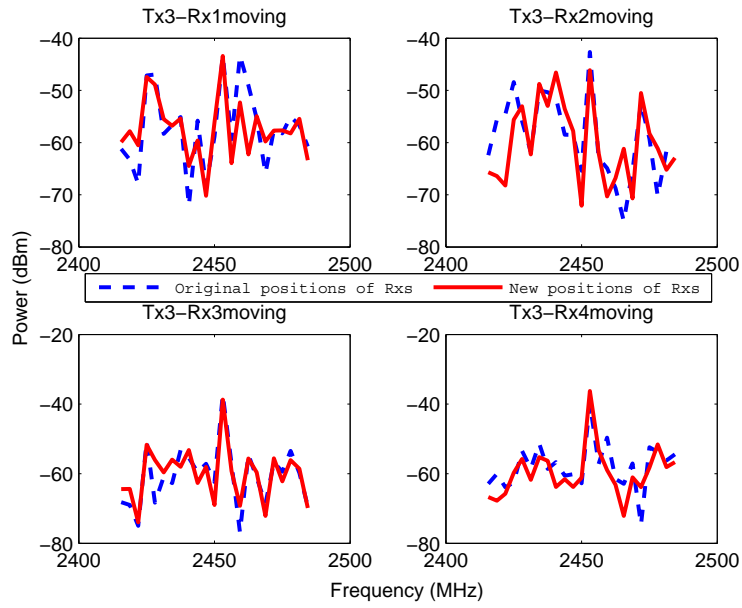


Figure 18: The comparison of the bandwidth dependency variations of the fading characteristics of the links between the Tx3 and the Rx1-4 when moving the Rxs with 2cm.

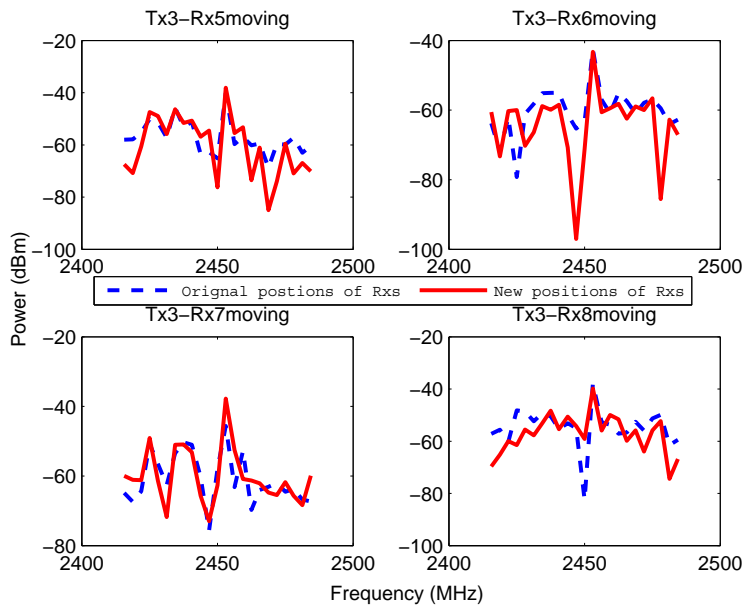


Figure 19: The comparison of the bandwidth dependency variations of the fading characteristics of the links between the Tx3 and the Rx5-8 when moving the Rxs with 2cm.

while ray tracing is incapable due to its limited number of rays. Moreover, the capability of simulating wide band fast fading characteristics by the MR-FDPF method can help wireless network planning to know the behavior of the wide band channel at any locations of the scenario.

In the future, we could further verify our simulation results by compared with measurements in other scenarios. And also the wide band fading characteristics in 3 dimensions (3D) is worth investigating by the 3D extension of the MR-FDPF method [18] [19]. We will also compare the wide band simulation by running N narrow band simulations with the simplified wide band MR-FDPF method [15]. Finally more other fading parameters extracted by the wide band simulation of the MR-FDPF method will be compared with measurements.

4 Conclusion

The MR-FDPF method is a finite difference based deterministic channel model with its complexity greatly reduced by using the multi-resolution structure. It is proved to be accurate and efficient in predicting large scale pathloss. Here in this report we tackle the small scale fadings based on the MR-FDPF method. The results verify that the MR-FDPF method is also capable of simulating the small scale fadings.

For the next step, we will work on investigating the possibility of proposing a combined channel model, in which the large scale fadings can be directly determined by the MR-FDPF method, while the small scale fadings will be determined by statistical models. We believe that a combined channel model would be a better choice in order to comprehensively describe radio channels in the real world.

Bibliography

- [1] J.-M. Gorce, K. Jaffres-Runser, and G. de la Roche, "Deterministic approach for fast simulations of indoor radio wave propagation," *Antennas and Propagation, IEEE Transactions on*, vol. 55, no. 3, pp. 938–948, 2007.
- [2] G. de la Roche, K. Jaffres-Runser, and J.-M. Gorce, "On predicting in-building wifi coverage with a fast discrete approach," *International Journal of Mobile Network Design and Innovation*, vol. 2, pp. 3–12, 2007.
- [3] P. Luthi, "Lattice wave automata: from radio wave to fracture propagation," Ph.D. dissertation, PhD thesis, Computer Science Department, University of Geneva, 24 rue General-Dufour, 1211 Geneva 4, Switzerland, 1998, 1998.
- [4] G. Durgin, "Theory of stochastic local area channel modeling for wireless communications," Ph.D. dissertation, Citeseer, 2000.
- [5] B. Fleury, M. Tschudin, R. Heddergott, D. Dahlhaus, and K. Ingeman Pedersen, "Channel parameter estimation in mobile radio environments using the sage algorithm," *Selected Areas in Communications, IEEE Journal on*, vol. 17, no. 3, pp. 434–450, Mar. 1999.
- [6] G. Durgin, *Space-time wireless channels*. Prentice Hall, 2003.
- [7] G. de La Roche and C. C. Chong, "Bandwidth Dependency Channel Model: On the Impact to Carrier Aggregated Systems," in *IEEE Wireless Communications and Networking Conference (WCNC 2011)*, Cancun, Mexico, March 2011.
- [8] W. Malik, B. Allen, and D. Edwards, "Bandwidth-dependent modelling of smallscale fade depth in wireless channels," *IET Microwaves, Antennas and Propagation*, vol. 2, pp. 519–528, 2008.
- [9] A. Valcarce, G. de la Roche, L. Nagy, J.-F. Wagen, and J.-M. Gorce, "Finite Difference Methods: A New Trend in Propagation Prediction," *IEEE Vehicular Technology Magazine, Special issue on Trends in Mobile Radio Channels*, June 2011.
- [10] N. Czink, B. Bandemer, G. Vazquez-Vilar, A. Paulraj, and L. Jalloul, "July 2008 radio measurement campaign: Measurement documentation," Stanford University, Smart Antennas Research Group, Tech. Rep., July 2008.
- [11] "Rusk medav channel sounders," 2008, [Online]. Available: <http://www.channelsounder.de>.

- [12] J.-M. Gorce, K. Jaffres-Runser, and G. de la Roche, "Deterministic approach for fast simulations of indoor radio wave propagation," *IEEE Transactions on Antennas and Propagation*, vol. 55, pp. 938–942, March 2007.
- [13] K. Runser and J.-M. Gorce, "Assessment of a new indoor propagation prediction method based on a multi-resolution algorithm," in *Vehicular Technology Conference, 2005. VTC 2005-Spring. 2005 IEEE 61st*, vol. 1, 2005, pp. 35 – 38 Vol. 1.
- [14] D. Jones, C. Perttunen, and B. Stuckman, "Lipschitzian optimization without the Lipschitz constant," *Journal of Optimization Theory and Applications*, vol. 79, no. 1, pp. 157–181, 1993.
- [15] J.-M. Gorce, G. Villemaud, and P. Flipo, "On Simulating Propagation for OFDM/MIMO Systems with the MR-FDPF Model," *Proceedings of the Fourth European Conference on Antennas and Propagation (EuCAP)*, pp. 1–5, April 2010.
- [16] G. de la Roche, X. Gallon, J.-M. Gorce, and G. Villemaud, "On predicting fast fading strength from indoor 802.11 simulations," in *Electromagnetics in Advanced Applications, 2007. ICEAA 2007. International Conference on*, 2007, pp. 407 –410.
- [17] M. Luo, D. Umansky, G. Villemaud, M. Lafort, and J.-M. Gorce, "Estimating channel fading statistics based on radio wave propagation predicted with deterministic mrfdpf method," in *Antennas and Propagation, 2011. EuCAP 2011. 5rd European Conference on*, 2011.
- [18] G. de la Roche and J.-M. Gorce, "A 3d formulation of mr-fdpf for simulating indoor radio propagation," in *Antennas and Propagation, 2006. EuCAP 2006. First European Conference on*, 2006, pp. 1 –6.
- [19] G. de la Roche, J.-M. Gorcey, and J. Zhang, "Optimized implementation of the 3d mr-fdpf method for indoor radio propagation predictions," in *Antennas and Propagation, 2009. EuCAP 2009. 3rd European Conference on*, 2009, pp. 2241 –2245.